Where cone snails and spiders meet: design of small cyclic sodium-channel inhibitors

Steve Peigneur[1,5], Olivier Cheneval[2], Mohitosh Maiti[3], Enrico Leipold[4], Stefan H. Heinemann[4], Eveline Lescrinier[3], Piet Herdewijn[3], Maria Elena De Lima[5,6], David J. Craik[2], Christina I. Schroeder[2*], Jan Tytgat[1*]

[1]Toxicology and Pharmacology, University of Leuven (KU Leuven), Campus Gasthuisberg, PO Box 922, Herestraat 49, 3000 Leuven, Belgium.

[2]Institute for Molecular Bioscience, The University of Queensland, Brisbane, Queensland, 4072, Qld, Australia.

[3]Laboratory of Medicinal Chemistry, Rega Institute for Medical Research, KU Leuven, Minderbroedersstraat 10, 3000 Leuven, Belgium.

[4]Department of Biophysics, Center for Molecular Biomedicine, Friedrich Schiller University Jena & Jena University Hospital, 07745 Jena, Germany.

[5]Laboratório de Venenos e Toxinas Animais, Dept de Bioquímica e Imunologia, Instituto de Ciências Biológicas, Universidade Federal de Minas Gerais, 31270-901, Belo-Horizonte, MG, Brazil.

[6] Programa de Pós-graduação em Ciências da Saúde, Biomedicina e Medicina, Instituto de Ensino e Pesquisa da Santa Casa de Belo Horizonte, Grupo Santa Casa de Belo Horizonte, Belo Horizonte, MG, Brazil.

*Address for correspondence: jan.tytgat@pharm.kuleuven.be (tel. +32 16 32 34 04; fax +32 16 3 23405) and c.schroeder@imb.uq.edu.au (tel. +61 7 334 62021).

Running Title: design of small cyclic sodium-channel inhibitors

Nonstandard Abbreviations

Nav; voltage gated sodium channel

TTX; tetrodotoxin

PnTx1; *Phoneutria nigriventer* toxin 1

KIIIA; *Conus kinoshitai* toxin IIIA

Abstract

A thirteen amino acid residue voltage-gated sodium channel (Na_V) inhibitor peptide, Pn, containing two disulfide bridges was designed using a chimeric approach based on a common pharmacophore deduced from sequence and secondary structural homology of two Na_V inhibitors; KIIIA, a 14-residue cone snail peptide with three disulfide bonds, and PnTx1, a 78-residue spider toxin with seven disulfide bonds. Like the parent peptides, this novel Na_V channel inhibitor was active on $Na_V1.2$. Through the generation of three series of peptide mutants, we investigated the role of key residues and cyclisation and their influence on Na_V inhibition and subtype selectivity. Cyclic PnCS1, a ten-residue peptide, cyclized via a disulfide bond, showed increased inhibitory activity towards therapeutically relevant Na_V channel subtypes including $Na_V1.7$ and $Na_V1.9$ while displaying remarkable serum stability. These peptides represent the first and the smallest cyclic peptide Na_V modulators to date and are promising templates for development of toxin-based therapeutics.

Key Words: voltage-gated sodium channel; spider toxin; cone snail toxin; peptide cyclisation; toxin-based therapeutics

Introduction

Voltage-gated sodium channels (Na_V) are integral membrane glycoproteins responsible for generation and propagation of action potentials in excitable cells. Mutations in genes encoding these channels can lead to a variety of severe illnesses. Na_V channels are considered as potential drug targets for diseases including pain syndromes, cardiac disorders and epilepsy (1, 2) asking for potent and selective Na_V channel inhibitors. *Phoneutria nigriventer*, also known as the Brazilian wandering spider, produces a potent venom, which is accountable for many of South Brazil's most severe envenomations in humans.(3, 4) *Phoneutria nigriventer* toxin 1 (PnTx1 or Mu-ctenitoxin-Pn1a following the nomenclature suggested by King and colleagues(5)) is a 78-amino acids residue peptide, comprising 14 cysteine residues. It has been characterized as a Na_V channel blocker with nM affinities for subtype $Na_V1.2$.(6-9) Recombinantly produced PnTx1 (rPnTx1) features selectivity toward neuronal Na_V channels with the following rank: $Na_V1.2$ > $Na_V1.7$ ~ $Na_V1.4$ > $Na_V1.3$ > $Na_V1.6$ > $Na_V1.8$.(10) No significant effect was observed for the cardiac isoform ($Na_V1.5$) and invertebrate channels.(10) PnTx1's inhibitory activity for $Na_V1.7$ channels is particularly important because of this Na_V channel subtype is essential for the transmission of acute and inflammatory pain signals.(10-12) Despite its interesting pharmacological profile, PnTx1 has never been explored for its therapeutically potential. Most likely this is because of large peptides are hard to administer and normally highly immunogenic.

Compared with these spider toxins, μ-conotoxins from predatory cone snails appear to have better properties: they have a small molecular size (<3 kDa), are readily synthesized, and display high selectivity for various Na_V channel subtypes.(13, 14) The μ-conotoxins possess an inhibitory cysteine knot structure containing three disulfide bridges. KIIIA, a 16-amino acid residue peptide isolated from the venom of *Conus kinoshitai*,(15, 16) targets a variety of Na_V channel subtypes with high affinity (5-300 nM half-blocking concentrations) and its structure-function relationship is well characterized.(15) KIIIA competes with the prototypic Na_V channel blocker tetrodotoxin (TTX), which inhibits the Na^+ flow through the channel by binding to the outer vestibule of the ion-conducting pore. Interestingly, despite the fact that KIIIA competes with TTX, their binding sites are not identical, but overlapping leading to a synergistic and antagonistic interactions between tetrodotoxin and μ-conotoxins in blocking Na_V channels.(17, 18) Alanine scanning mutagenesis and further structure-activity studies of KIIIA have shown that residues on the C-terminal α helix, including K7, W8, R10, D11, H12 and R14, are functionally important(15, 19-21) (Fig. 1c). Moreover, alanine replacement of K7, W8 and D11 yields more selective blockers, discriminating between neuronal ($Na_V1.2$) and skeletal ($Na_V1.4$) Na_V channels.(22, 23) Comparing the sequence of both toxins, one can observe similarities between the functionally important segment of the 16-residue conotoxin KIIIA with a central segment of the 78-residue spider toxin PnTx1 (Fig. 1d). This apparent homology raises the question whether it is possible to confer pharmacological properties of the large spider toxins to the scaffold of a miniaturized cone snail toxin.

Material & Methods

Peptide synthesis

Pn and PnM1-PnM9 were purchased from GenicBio Limited®. PnCS1-PnCS4 were chemically synthesized using standard Fmoc solid-phase synthesis protocols on a Symphony peptide synthesizer (Protein Technologies Inc). PnCS1 and PnCS2 were assembled on rink-amide resin at 0.25 mmol scale to produce an amidated C terminus whereas PnCS3 and PnCS4 were assembled on 2-chlorotrityl (2-CTC) resin at 0.25 mmol scale. Amino-acid protecting groups used were Cys(Trt), Asp(tBu), Lys(Boc), Asn(Trt), Arg(Pbf), Trp(Boc), Lys(Alloc) and Asp(Allyl). For PnCS1, the peptide was released from the resin and amino acid side chain simultaneously deprotected by incubation with triisopropylsilane (TIPS):H_2O:trifluoroacetic acid (TFA) (2:2:96, v/v/v) for 2.5 h at room temperature. TFA was evaporated under vacuum, and the peptide precipitated with ice-cold diethyl ether. PnCS1 was dissolved in 50% acetonitrile (ACN) (0.05% TFA) and lyophilized. The crude linear peptide was purified using reversed phase high-performance liquid chromatography (RP-HPLC) (0–80% B over 80 min, flow rate 8 mL/min, solvent A; 0.05% TFA, solvent B 90% ACN/0.045% TFA on a Shimadzu instrument) and its molecular mass determined using electrospray mass spectrometry (ESI-MS). Purified PnCS1 was oxidized at room temperature in 0.1 M ammonium bicarbonate buffer at pH 8.3 over 24 h. Peptides were >95% pure, as determined using analytical-HPLC, and 1D and 2D NMR ^{1}H spectroscopy was used to confirm the presence of one isomer. The PnCS2's lactam bridge was formed by cleaving the Allyl and Alloc groups off with 3 eq. of Pd(Ph3P)4 in chloroform/acetic acid/N-methylmorpholine (37:2:1) for 2 h under argon. The resin was then consecutively washed with 0.5% N,N-diisopropylethylamine (DIPEA) in N,N-dimethylformamide (DMF) and sodium diethyldithiocarbamate (0.5% w/w) in DMF to remove the catalyst. The bond was then formed by coupling the two free side chains with 2 eq. of (benzotriazol-1-yloxy)tris(dimethylamino)phosphonium hexafluorophosphate (BOP) and 4 eq. of DIPEA in DMF overnight. The resin was washed with DMF and then dichloromethane (DCM) before being dried under N_2. The peptide was then worked up as previously described for PnCS1. For PnCS3 and PnCS4, the peptides were released from the resin by treatment of 1% TFA in DCM for 10 x 5 min leaving the protecting groups attached. PnCS3 and PnCS4 were cyclized protected in solution by addition of (1-[bis(dimethylamino)methylene]1H1,2,3triazolo[4,5b]pyridinium3oxidhexafluorophosphate) (HATU) and DIPEA to peptide (ratio 5:10:1) in DMF for 3 h. The protecting groups were subsequently removed using the conditions described for cleavage of PnCS1 and PnCS2. PnCS4 was oxidized as previously described and both PnCS3 and PnCS4 were purified and characterized as described above.

NMR spectroscopy

1D and 2D NMR spectra of Pn were recorded on a 600 MHz or 500 MHz Bruker Avance II NMR spectrometer equipped with a cryoprobe. Peptide samples were prepared in 90% H_2O/10% D_2O or 100% D_2O (Sigma-Aldrich) at ~5 mM and pH ~4. Water suppression was achieved using excitation sculpting gradients.(42) Spectra recorded were 1D ^1H and 2D TOCSY (mixing time 80 ms), NOESY (mixing time 200 and 300 ms) and DQF-COSY. In the processing of two-dimensional spectra, data were apodized with a shifted sine-bell square function in both dimensions. All spectra were processed by using Topspin 2.1 (Bruker Biospin) and analyzed using CARA program (version 1.8.4). Proton chemical shifts were calibrated by using residual water (HOD) signal as a reference (4.97 ppm at 293 K). Natural abundance ^1H-^{13}C HSQC spectra in D_2O were recorded with sensitivity enhancement and gradient coherence selection, optimized for selection of aliphatic CH groups (JCH = 135 Hz) using 64 scans, 1024/2048 complex data points, and 12072/7210 Hz spectral widths in t1 and t2 respectively.

Structural constraints

Distance restraints were derived from cross-peak volumes of the NOESY spectrum recorded with 200 ms mixing time. Average cross-peak volume of the geminal methylene proton pairs was used as reference volume, which corresponds to the fixed reference distance of 1.8 Å. The $^3J_{HN\text{-}H\alpha}$ coupling constants were measured from the one-dimensional proton spectrum recorded in H_2O and then should be converted to dihedral restraints as follows: $^3J_{HN\text{-}H\alpha} > 8$ Hz, $\varphi = -120 \pm 30^o$; $^3J_{HN\text{-}H\alpha} < 5.5$ Hz $= -60 \pm 30^o$. However, all $^3J_{HN\text{-}H\alpha}$ were between 5.5 and 8 Hz, therefore no dihedral restraints were applied in the structure calculation.

Structure calculations

All structure calculations were performed by using Xplor-NIH program, version 2.25. A set of 100 structures was generated by torsion angle molecular dynamics, starting from an extended strand and by using NMR-derived NOE restraints and two disulfide (C1-C11, C3-C13) bond restraints. Following torsion angle molecular dynamics, the majority of the structures had no NOE or dihedral violations. Twenty lowest energy structures were used for further refinement during a “gentle molecular dynamics” round in explicit water.(43) A box of water was constructed and optimized around selected structures obtained from the previous torsion angle dynamics step. The final stage of refinement commenced with a 20-ps constant temperature molecular dynamics simulation at 300 K (20,000 steps of 0.001 ps) and was followed by a 200-step conjugate gradient energy minimization of the average structure of the last 10 ps of the 20 ps simulation. Structures were analyzed by using PROCHECK. Visual representations of the molecule were created by using UCSF Chimera program (version 1.8rc).

Expression of voltage-gated ion channels in Xenopus laevis oocytes

For the expression of Na_V channels (hNa_V1.1, rNa_V1.2, rNa_V1.3, rNa_V1.4, hNa_V1.5, mNa_V1.6, rNa_V1.7, rNa_V1.8, hNa_V1.9_C4, the invertebrate channels DmNa_V1, BgNa_V1.1, VdNa_V1 and the auxiliary subunits rβ1, hβ1 and TipE) in *Xenopus* oocytes, the linearized plasmids were transcribed using the T7 or SP6 mMESSAGE-mMACHINE transcription kit (Ambion®, Carlsbad, California, USA). The construction of Na_V1.9_C4 was described previously.(33) The harvesting of stage V-VI oocytes from anaesthetized female *X. laevis* frog was previously described(44) with a protocol adjustment in which the frogs are anesthetized by placement in 0.1% Tricaine (amino benzoic acid ethyl ester, Sigma®) solution. Oocytes were injected with 50 nL of cRNA at a concentration of 1 ng/nL using a micro-injector (Drummond Scientific®, Broomall, Pennsylvania, USA). The oocytes were incubated in a solution containing (in mM): NaCl, 96; KCl, 2; $CaCl_2$, 1.8; $MgCl_2$, 2 and HEPES, 5 (pH 7.4), supplemented with 50 mg/L gentamycin sulfate.

Electrophysiological recordings

Two-electrode voltage-clamp recordings were performed at room temperature (18–22 °C) using a Geneclamp 500 amplifier (Molecular Devices®, Downingtown, Pennsylvania, USA) controlled by a pClamp data acquisition system (Axon Instruments®, Union City, California, USA). Whole-cell currents from oocytes were recorded 1–4 days after mRNA injection. Bath solution composition was (in mM): NaCl, 96; KCl, 2; $CaCl_2$, 1.8; $MgCl_2$, 2 and HEPES, 5 (pH 7.4). Voltage and current electrodes were filled with 3 M KCl. Resistances of both electrodes were kept between 0.8 and 1.5 MΩ. The elicited currents were filtered at 1 kHz and sampled at 20 kHz using a four-pole low-pass Bessel filter. Leak subtraction was performed using a -P/4 protocol. In order to avoid overestimation of a potential toxin-induced shift in the current–voltage relationships of inadequate voltage control when measuring large Na^+ currents in oocytes, only data obtained from cells exhibiting currents with peak amplitude below 2 μA were considered for analysis. For the electrophysiological analysis of toxins, a number of protocols were applied from a holding potential of −90 mV with a start-to-start interval of 0.2 Hz. Na^+ current traces were evoked by 100-ms depolarizations to Vmax (the voltage corresponding to maximal Na^+ current in control conditions). The current–voltage relationships were determined by 50-ms step depolarizations between −90 and 70 mV, using 5-mV increments. The Na^+ conductance (gNa) was calculated from the currents according to Ohm's law: $gNa = INa/(V - V_{rev})$, where INa represents the Na^+ current peak amplitude at a given test potential V, and V_{rev} is the reversal potential. The values of gNa were plotted as a function of voltage and fitted using the Boltzmann function: $gNa/gmax = [1+(\exp(Vg-V)/k)]^{-1}$, where g_{max} represents maximal gNa, Vg is the voltage corresponding to half-maximal conductance and k is the slope factor. Toxin-induced effects on the steady-state inactivation were investigated using a standard two-step protocol. In this protocol, 100-ms conditioning 5-mV step prepulses ranging from −90 to 70 mV were followed by a 50-ms test pulse to −30 or −10 mV. Data were normalized to the maximal Na^+ current amplitude, plotted against prepulse potential and fitted using the Boltzmann function: $INa/Imax = [(1-C)/(1+\exp((V-Vh)/k))]+C$, where Imax is the maximal

INa, Vh is the voltage corresponding to half-maximal inactivation, V is the test voltage, k is the slope factor, and C is a constant representing a non-inactivating persistent fraction (close to zero in control). The time constants (τ) of the Na_V channel fast inactivation were measured directly from the decay phase of the recorded Na^+ current using a single-exponential fit. To assess the concentration–response relationships, data were fitted with the Hill equation: $y = 100/[1+(EC_{50}/[toxin])^h]$, where y is the amplitude of the toxin-induced effect, EC_{50} is the toxin concentration at half maximal efficacy [toxin], is the toxin concentration and h is the Hill coefficient. All data are presented as mean ± standard error (S.E.M.) of at least 5 independent experiments ($n \geq 5$). All data were tested for normality using a D'Agustino Pearson omnibus normality test. All data were tested for variance using Bonferroni test or Dunn's test. Data following a Gaussian distribution were analyzed for significance using one-way ANOVA. Non-parametric data were analyzed for significance using the Kruskal–Wallis test. Differences were considered significant if the probability that their difference stemmed from chance was 55% ($p < 0.05$). All data was analyzed using pClamp Clampfit 10.0 (Molecular Devices®, Downingtown, Pennsylvania, USA) and Origin 7.5 software (Originlab®, Northampton, Massachusetts, USA).

Serum-stability tests

The stability of peptides in human serum was examined using a protocol reported previously.(45) Briefly, stock solutions of peptides (300 μM) were diluted 10 times with pre-warmed 100% human serum isolated from male AB plasma (Sigma-Aldrich) and incubated at 37 °C for 0, 1, 2, 3, 5, 8, 12 and 24 h. Controls with peptides in ND96 were included. The reaction was stopped by denaturing the serum proteins with urea at a final concentration of 3 M at 4 °C for 10 min, followed by precipitation of serum proteins with trichloroacetic acid at a final concentration of 7% (v/v) (4 °C, 10 min) and centrifugation (17,000 g, 10 min). The supernatant of each sample was recovered and run on an analytical column using a linear gradient of 0–40% solvent B (acetonitrile 100% (v/v) with 0.085% (v/v) TFA in H_2O) in solvent A (0.1% (v/v) TFA in H_2O) over 40 min at a flow rate of 0.5 mL/min with monitoring at 214 nm. The elution profile of each peptide was identified by the ND96 sample from 0 time point. The percentage of peptide remaining in serum-treated samples was determined by comparing the height of the peptide peak obtained at each time point with that of the peptide peak obtained at 0 time point. Each experiment was done in triplicate.

Results

We subsequently designed a 13-amino acids residue peptide with two disulfide bridges incorporating residues from the central segment of PnTx1 and known pharmacophore resides from KIIIA (Fig. 1b). This hybrid peptide, Pn, showed an interesting selectivity pattern when screened against a panel of Na_V channel subtypes. A first series of Pn mutants (PnM1-PnM4) and a subsequent second series (PnM5-PnM9) allowed us to pinpoint

the key residues important for activity. The remarkable ribbon-shaped and cysteine-stabilized conformation inspired the design of a third series of cyclic peptides incorporating various cyclisation strategies, including backbone, lactam bridge and disulfide bond cyclisation, with retained potent activity. These cyclized Na_V channel inhibitor peptides are the smallest cyclic peptides reported to inhibit Na_V channel to date and represent promising templates for further development of toxin-based therapeutics with improved physiochemical properties.

Design strategy

In this study, we aimed to design minimized hybrid peptides inhibiting Na_V channels, benefiting from features known to be important for Na_V inhibition of two toxins, KIIIA and PnTx1. Alignment of PnTx1 and KIIIA shows that the spacing of key residues of KIIIA (W8, R10 and R14) is conserved in PnTx1 (W33, R35 and K39) (Fig. 1d). Previous work has illustrated that the first disulfide bridge between Cys1 and Cys9 in KIIIA is removable, almost without affecting the peptides inhibitory potency on $Na_V1.2$ and $Na_V1.4$.(19, 24) Hence, in order to simplify peptide synthesis, the first disulfide bridge was excluded in our hybrid peptide. This resulted in the design of a thirteen amino acids residue peptide with two disulfide bridges possessing the central segment of PnTx1 while simultaneously incorporating key residues from KIIIA grafted onto the scaffold of a minimized KIIIA peptide.

Solution structure of Pn

Analysis of one-dimensional (1D) and two-dimensional (2D) TOCSY, NOESY, DQF-COSY and ^{1}H-^{13}C HSQC NMR spectra shows the formation of a predominant single set of sharp resonances for the Pn peptide, indicating that it adopts a single conformation in solution. However, additional NOEs were observed for the HE1 protons of the W6 and W9 side chains in the NOESY and TOCSY spectra, albeit with lower intensity, suggesting tryptophan side chain flexibility and the presence of a minor side chain conformation.

Resonance assignment was performed using homonuclear 2D TOCSY, NOESY and DQF-COSY spectra by following standard assignment protocols as outlined by Wüthrich.(25) Assignment of ^{1}H-^{13}C HSQC spectra further reconfirmed the homonuclear proton assignments. The geminal methylene protons were not assigned stereospecifically, and the NOE distance restraints involving these protons were used ambiguously during structure calculation in the Xplor-NIH program. The solution structure of Pn was calculated using 124 distance (78 intra-residue and 46 inter-residue) restraints derived from NOESY spectra including two disulfide (C1–C11, C3–C13) bond restraints. All $^{3}J_{HN\text{-}H\alpha}$ coupling constant values were in between 5.5 and 8 Hz, indicating angular averaging across the Φ dihedrals reflecting flexibility in the peptide backbone. Therefore, no dihedral restrains were included during structure calculation. Moreover, temperature coefficients ($\Delta\delta/\Delta T$) derived from the

chemical shifts of backbone amide protons were –3 to –8 ppb/K, with only one exception being residue C11 with a value of –1 ppb/K. Typically, residues with temperature coefficients <–4.6 ppb/K are considered shielded and potentially involved in a hydrogen bond. No hydrogen bond acceptors were identified during structure calculations and, therefore, no hydrogen bond restrains were included in the structure calculations. Statistical analysis was carried out on the final ensemble of 20 lowest energy structures (Fig. 1a, Table 1) of synthetic peptide Pn. The final 20 structures are very flexible with backbone and heavy atom RMSD of 2.89 ± 1.16 and 4.35 ± 1.15, respectively, calculated using Molmol. Evaluation of the structure with PROCHECK showed no bad non-bonded contacts and the majority of the backbone dihedral angles were within the allowed regions of the Ramachandran plot (3.1% in the disallowed region). A closer look into the structures of Pn reveals that the peptide backbone adopts a flexible, cyclic ribbon-shaped conformation (Fig. 1a), having a main disordered loop that is closed by two disulfide bonds (C1–C11 and C3–C13). The structure is devoid of any α-helical or β-turn secondary structural elements. Side-chain orientations for all residues vary considerably within different defined domains.

PnCS1-PnCS4 peptides were analyzed using 1D ^{1}H and 2D TOCSY and NOESY spectra. All peptides displayed one single conformation evident from one set of resonances present for each peptide.

Electrophysiological characterization of Pn and mutants

When screened against a panel of ten different Na_V channel isoforms ($Na_V1.1$–1.8, and Na_V insect channels $BgNa_V1.1$, VNa_V1), we found that 50 µM of Pn selectively inhibited 44.6 ± 2.4% ($n\geq9$) of the $Na_V1.2$ channel (Fig. 2) and a concentration-response curve produced an IC_{50} value of 53.7 ± 3.2 µM (Fig. 3b). No shift in the voltage dependence of activation or steady-state inactivation was observed after addition of 50 µM Pn (Fig. 3a). To verify that Pn does bind to neurotoxin site 1, competitive binding experiments were performed using both mother molecules, KIIIA or PnTx1, as competitors. Application of PnTx1 at its IC_{50} value of 35 nM (10) resulted in 48.7 ± 4.3% ($n\geq8$) inhibition of the Na^+ peak current. Subsequent addition of IC_{50} concentrations of Pn did not result in further inhibition (Fig. 3b). Similar experiments, in which first IC_{50} concentration of KIIIA (60 nM(26)) was applied, followed by subsequently addition of IC_{50} of Pn, also did not result in additional current reduction (data not shown), indicating that Pn binds to site 1, like its parent peptides PnTx1 and KIIIA.

In order to improve potency of Pn, we designed a first series of mutants (Series 1) using data available from structure-function studies on KIIIA and other µ-conotoxins (Fig. 1d).(19, 20, 27-31) From this first series of mutants, PnM2 showed the most promising increase in activity when tested on $Na_V1.2$-$Na_V1.6$ (Table 2). Compared to Pn, PnM2 has the G4 and G5 replaced by arginines, and the lysine between the two last cysteines has been removed, shortening the peptide by one residue. The second series of mutants (Series 2, Fig. 1d) was

designed based on the PnM2 sequence. Of these mutants, PnM9 was the most potent displaying an IC_{50} value for $Na_V1.2$ channels of 312.4 ± 12.8 nM (Fig. 4b, Table 2). In PnM9, Gly7 was replaced by an alanine since it has been reported that a glycine at this position is unfavorable for Na_V channel activity ($Na_V1.1$-$Na_V1.7$).(32) Furthermore, an extra positive charge in form of Arg11, was introduced prior to the C-terminal cysteine. Although PnM9 increased in potency at $Na_V1.2$ compared to Pn and PnM2, it was less selective and also inhibited the current through $Na_V1.4$ channels, while being inactive against $Na_V1.5$ and $Na_V1.6$ channels (Fig 4a, Table 2).

Considering the close proximity of the N and the C terminus in the NMR structure of Pn (Fig. 1a), and the improved potency of PnM9 compared to Pn, a third series of peptides, PnCS1-PnCS4 was designed (Series 3, Fig. 1d). In PnCS1, the second disulfide bond was removed and the peptide was cyclized via its N- and C-terminal Cys residues, resulting in a ten-amino acid residue peptide. In PnCS2, the peptide was also shortened with respect to PnM9 and the N- and C-terminal Cys residues were replaced with an Asp and a Lys residue, respectively, and cyclized via a lactam bridge, resulting in a ten-amino acid residue peptide. Both PnCS1 and PnCS2 included a C-terminal amidation. PnCS3 was backbone cyclized following the replacement of the N- and C-terminal Cys residues with Ala and Gly, respectively, again leading to a ten-residue peptide, whereas in PnCS4 an additional Gly was introduced in both the N- and the C-terminal and the peptide was backbone cyclized via an amide bond, resulting in a 15-residue peptide. Peptides, PnCS1-PnCS4, were tested for their activity against nine vertebrate Na_V channels ($Na_V1.1$-$Na_V1.9$_C4) and three invertebrate Na_V channel subtypes ($BgNa_V1.1$, $VdNa_V1$ and $DmNa_V1$) (Fig. 5). The concentration-dependence inhibitory effect of the PnCS peptides on Na_V channels and IC_{50} values for the four cyclic variants are shown in Table 3. Both PnCS2 and PnCS3 showed a strong reduction in potency, while PnCS1 and PnCS4 were active with IC_{50} values in an approximately 3-fold higher range (Table 3). PnCS1 was used to further investigate the mechanism in which these cyclic peptides interact with their target. PnCS1, at a concentration of 1 µM, significantly inhibited the current through TTX-sensitive channels ($Na_V1.1$-$Na_V1.4$, $Na_V1.6$ and $Na_V1.7$), while the TTX-resistant isoforms were less ($Na_V1.5$ and $Na_V1.9$_C4) or not sensitive ($Na_V1.8$) (Fig. 5). $Na_V1.9$_C4 is a chimera of $Na_V1.9$ harboring the C-terminus of $Na_V1.4$. Previous work has shown that the C-terminal structure of $Na_V1.9$ is limiting the heterologous expression in host cells, thus replacing the C-terminus with the corresponding segment of the $Na_V1.4$ channel allows for functional expression in oocytes.(33) Interestingly, this chimera retains the same sensitivity for site-1 blockers as $Na_V1.9$.(33) $Na_V1.4$ channels were used to further characterize the interaction of 1 µM PnCS1 with the channel. Steady-state activation and inactivation curves show that no modulation of Na_V channels occurs upon peptide binding (Fig. 6a, b). The midpoint of activation for $Na_V1.4$ did not shift significantly since the $V_{1/2}$ values of activation yielded –27.4 ± 0.1 mV in control and –28.6 ± 0.3 mV in the presence of PnCs1. For the inactivation curves, the $V_{1/2}$ shifted from –59.4 ± 0.6 mV to –57.9 ± 1.4 mV in

control and toxin situation, respectively. PnCS1 did not significantly enhance the recovery from inactivation (Fig. 6c). PnCs1 inhibition was found to be voltage independent since no difference in the degree of inhibition was observed over a range of test potentials (Fig. 6d). To investigate the state-dependence of inhibition, the following protocol was used. As control, a series of depolarizing pulses was applied to an oocyte expressing $Na_V1.4$ channels. Thereafter, 0.5 µM PnCS1 was added and no pulsing performed for 2 min. This was followed by a similar series of pulses. A strong degree of delay of inactivation was observed after the 2 min incubation, indicating that the open state is not required for toxin interaction with the channel (Fig. 6e).

Serum stability test

To evaluate whether the designed cyclic peptides acquire increased stability compared to the non-cyclized peptides, linear and folded non-cyclic peptides (Pn, PnM9) and cyclic peptides (PnCS1-4) were incubated in human serum and the remaining peptide was quantified by analytical-HPLC (Fig. 7). Linear Pn and PnM9 were fully degraded by proteases in serum within 1 h. The oxidized peptides showed higher stability than linear peptides. Nevertheless, after 24 h folded Pn was completely degraded whereas only 16% of PnM9 remained. In contrast, the cyclic peptides PnCS1-CS4 were stable in human serum with 100% of peptide remaining after 24h.

Discussion

The initial goal of this study was to identify small cyclic inhibitors for Na_V subtypes. Therefore, we grafted the proposed pharmacophore of PnTx1, a potent Na_V channel inhibitor peptide toxin from the Brazilian wandering spider, into the scaffold of KIIIA, a potent Na_V channel inhibiting peptide isolated from the venom of a cone snail. The resulting peptide, Pn, was investigated for Na_V channel inhibition. Competitive binding experiments suggest that Pn competes with its parent peptides, PnTx1 and KIIIA, for the same binding site on the Na_V channel. It can thus be assumed that Pn and analogs obstruct the ion flow by binding at the extracellular channel vestibule rather than acting as voltage-sensor modifiers. These results corroborate well with previous studies indicating that PnTx1 and µ-conotoxins compete for the same site as well.(6) The solution structure of the Pn peptide was determined using NMR displaying a highly flexible backbone and a minor set of peaks were observed for the HE1 protons of both Trp residues in the 1D proton NMR spectra suggesting the presence of a minor conformation.

Next, two series of peptide mutants were designed in order to increase the potency of Pn, resulting first in PnM2 and subsequently in PnM9, the latter displaying nM inhibition at Na_V channel subtypes $Na_V1.2$ and $Na_V1.4$. A third series of peptides was designed with the aim to further minimize the peptide scaffold as well as introduce improved stability of the peptides through various methods of cyclisation including disulfide and lactam bond as well as backbone cyclisation. Within the third series of peptides, PnCS1 retained inhibition at submicromolar

potency while losing selectivity for $Na_V1.2$. Cyclization of PnCS1-PnCS4 rendered these peptides highly stable towards degradation when incubated in human serum, compared to linear or oxidized, but not cyclized peptides in this study, indicating a great improvement in their biopharmaceutical properties. However, due to the lack of selectivity for this series of peptides, future structure-function studies are required to obtain peptides with a Na_V channel subtype selective activity. . Interestingly, PnCS1, PnCS3 and PnCS4 showed inhibition of $Na_V1.9\_C4$, albeit in low μM range, an understudied Na_V channel due to difficulties relating to heterologous expression as well as the lack of potent and selective inhibitors. Nav1.9 is of particular interest due to its links to inflammatory mediated gut pain present in Chron's disease and irritable bowls syndrome (IBD).(34)

Considerable effort has been made in elucidating the molecular determinants for the subtype specificity of peptide toxins towards specific Na_V channel subtypes. More specific, many studies have focused on the key residues responsible for subtype selectivity among μ-conotoxins.(15, 35-39) These studies paved the way for the rational design of selective Na_V channel antagonists and will assist in further peptide engineering of the PnCS scaffold with the aim to design small, cyclic, selective and potent Na_V channel inhibitors for therapeutically relevant Na_V subtypes.

Drugs currently used in humans can roughly be divided in either small molecules or large biologics, including antibodies. Whereas small organic molecules tend to display the desirable physicochemical property of oral bioavailability, due to their size, small molecule drugs may suffer from reduced target selectivity that often ultimately manifests in unwanted side effects. Large biologics on the other hand, tend to be exquisitely specific for their targets due to their larger surface area. However, this usually comes at the cost of low bioavailability, poor membrane permeability, and metabolic instability.(40, 41) Peptides have emerged with the promise to bridge the gap between small molecules and large biologics, and the field of drug development is now refocusing its efforts to pursue peptides as lead molecules that fit between these two molecular weight extremes and at the same time, exhibit the advantageous characteristics of both.(40) Indeed, molecules combining advantages of small molecules (cost, conformational restriction, membrane permeability, metabolic stability, oral bioavailability) with those of large biologics (natural components, target specificity, high potency) might represent the novel tools to overcome the hurdles experienced today in drug discovery.(40) It is within this philosophy of combining the better of two worlds that we decided to combine the sophisticated evolutionary peptide chemistry of cone snails and spiders in order to design small, cyclic and bioactive peptides. The resulting peptides represent the first and the smallest (ten residues) cyclic Na_V modulators and are promising starting scaffolds for further development of peptide-based therapeutics.

In summary, this study has shown that it is possible to define peptide toxins targeting Na_V channels to a minimal pharmacophore and that cyclization of these minimized peptides can greatly enhance their

biopharmaceutical properties without influencing activity. The PnCS peptides represent a promising template for further design of lead compounds in the development of novel therapeutic agents for treatment of Na_V channel related diseases.

Acknowledgements

The authors thank John N. Wood (University College London, London, UK) for sharing rNa_V1.8; A. L. Goldin (University of California, Irvine, CA, USA) for sharing rNa_V1.1, rNa_V1.2, rNa_V1.3, and mNa_V1.6; G. Mandel (State University of New York, Stony Brook, NY, USA) for sharing rNa_V1.4; R. G. Kallen (Roche Institute of Molecular Biology, Nutley, NJ, USA) for sharing hNa_V1.5; K. Dong (Michigan State University, USA) for sharing the BgNa_V1.1 and VdNa_V1 clones; S. C. Cannon (University of Texas Southwestern Medical Center, Dallas, TX, USA) for sharing the hβ1 subunit and Martin S. Williamson (Rothhamsted Research, Harpenden, UK) for providing the Para and tipE clone. The Na_V1.7 clone was kindly provided by F. Bosmans (Johns Hopkins University, USA). This work was supported by the following grants: JT was supported by grant CELSA/17/047 – BOF/ISP. SP is a PhD fellow supported by CAPES (Coordenação de Aperfeiçoamento de Pessoal de Nível Superior). DJC is an Australian Research Council (ARC) Australian Laureate Fellow (FL150100146) and CIS is an Institute for Molecular Bioscience Industry Fellow and ARC Future Fellow (FT160100055). MEdL was supported by grants from CAPES (Coordenação de Aperfeiçoamento de Pessoal de Nível Superior), CNPq (Conselho Nacional de Desenvolvimento Científico e Tecnológico) and FAPEMIG (Fundação de Pesquisa do Estado de Minas Gerais).

Author Contributions

S. Peigneur, J. Tytgat, D.J. Craik, C.I. Schroeder designed the study. S. Peigneur carried out all electrophysiology and serum stability experiments, S. Peigneur, J. Tytgat and C.I. Schroeder designed the peptides. M. Maiti carried out NMR on Pn peptide and C.I. Schroeder carried out NMR on all other peptides. S. Peigneur and C.I. Schroeder wrote the manuscript and J. Tytgat, S.H. Heinemann, E. Leipold, P. Herdewijn, M.E. deLima and D.J. Craik assisted with writing and editing.

Competing Financial Interests statement

No competing financial interests to state.

References

1. Abdelsayed, M., and Sokolov, S. (2013) Voltage-gated sodium channels: pharmaceutical targets via anticonvulsants to treat epileptic syndromes. *Channels (Austin)* **7**, 146-152

2. Moreau, A., Gosselin-Badaroudine, P., and Chahine, M. (2015) Gating pore currents, a new pathological mechanism underlying cardiac arrhythmias associated with dilated cardiomyopathy. *Channels* **9**, 139-144

3. De Marco Almeida, F., de Castro Pimenta, A. M., Oliveira, M. C., and De Lima, M. E. (2015) Venoms, toxins and derivatives from the Brazilian fauna: valuable sources for drug discovery. *Sheng Li Xue Bao* **67**, 261-270

4. de Lima M. E., F. S. G., Alessandra Matavel, Kenia Pedrosa Nunes, Carolina Nunes da Silva, Flávia de Marco Almeida, Marcelo Ribeiro Vasconcelos Diniz, Marta Nascimento do Cordeiro, Maria Stankiewicz, Paulo Sérgio, Lacerda Beirão (2015) Phoneutria nigriventer Venom and Toxins: A Review. pp. 1-24, Springer, Dordrecht

5. King, G. F., Gentz, M. C., Escoubas, P., and Nicholson, G. M. (2008) A rational nomenclature for naming peptide toxins from spiders and other venomous animals. *Toxicon* **52**, 264-276

6. Martin-Moutot, N., Mansuelle, P., Alcaraz, G., Dos Santos, R. G., Cordeiro, M. N., De Lima, M. E., Seagar, M., and Van Renterghem, C. (2006) Phoneutria nigriventer toxin 1: a novel, state-dependent inhibitor of neuronal sodium channels that interacts with micro conotoxin binding sites. *Mol Pharmacol* **69**, 1931-1937

7. Diniz, M. R., Theakston, R. D., Crampton, J. M., Nascimento Cordeiro, M., Pimenta, A. M., De Lima, M. E., and Diniz, C. R. (2006) Functional expression and purification of recombinant Tx1, a sodium channel blocker neurotoxin from the venom of the Brazilian "armed" spider, Phoneutria nigriventer. *Protein Expr Purif* **50**, 18-24

8. Diniz, C. R., Cordeiro Mdo, N., Junor, L. R., Kelly, P., Fischer, S., Reimann, F., Oliveira, E. B., and Richardson, M. (1990) The purification and amino acid sequence of the lethal neurotoxin Tx1 from the venom of the Brazilian 'armed' spider Phoneutria nigriventer. *FEBS letters* **263**, 251-253

9. Diniz, M. R., Paine, M. J., Diniz, C. R., Theakston, R. D., and Crampton, J. M. (1993) Sequence of the cDNA coding for the lethal neurotoxin Tx1 from the Brazilian "armed" spider Phoneutria nigriventer predicts the synthesis and processing of a preprotoxin. *J Biol Chem* **268**, 15340-15342

10. Silva, A. O., Peigneur, S., Diniz, M. R., Tytgat, J., and Beirao, P. S. (2012) Inhibitory effect of the recombinant Phoneutria nigriventer Tx1 toxin on voltage-gated sodium channels. *Biochimie* **94**, 2756-2763

11. Liu, M., and Wood, J. N. (2011) The roles of sodium channels in nociception: implications for mechanisms of neuropathic pain. *Pain Med* **12 Suppl 3**, S93-99

12. King, G. F., and Vetter, I. (2014) No gain, no pain: NaV1.7 as an analgesic target. *ACS chemical neuroscience* **5**, 749-751

13. Tietze, A. A., Tietze, D., Ohlenschlager, O., Leipold, E., Ullrich, F., Kuhl, T., Mischo, A., Buntkowsky, G., Gorlach, M., Heinemann, S. H., and Imhof, D. (2012) Structurally diverse mu-conotoxin PIIIA isomers block sodium channel NaV 1.4. *Angew Chem Int Ed Engl* **51**, 4058-4061

14. Prashanth, J. R., Dutertre, S., and Lewis, R. J. (2017) Pharmacology of predatory and defensive venom peptides in cone snails. *Molecular bioSystems* **13**, 2453-2465

15. Zhang, M. M., Green, B. R., Catlin, P., Fiedler, B., Azam, L., Chadwick, A., Terlau, H., McArthur, J. R., French, R. J., Gulyas, J., Rivier, J. E., Smith, B. J., Norton, R. S., Olivera, B. M., Yoshikami, D., and Bulaj, G. (2007) Structure/function characterization of micro-conotoxin KIIIA, an analgesic, nearly irreversible blocker of mammalian neuronal sodium channels. *J Biol Chem* **282**, 30699-30706

16. Bulaj, G., West, P. J., Garrett, J. E., Watkins, M., Zhang, M. M., Norton, R. S., Smith, B. J., Yoshikami, D., and Olivera, B. M. (2005) Novel conotoxins from Conus striatus and Conus kinoshitai selectively block TTX-resistant sodium channels. *Biochemistry* **44**, 7259-7265

17. Zhang, M. M., McArthur, J. R., Azam, L., Bulaj, G., Olivera, B. M., French, R. J., and Yoshikami, D. (2009) Synergistic and antagonistic interactions between tetrodotoxin and mu-conotoxin in blocking voltage-gated sodium channels. *Channels (Austin)* **3**, 32-38

18. French, R. J., Yoshikami, D., Sheets, M. F., and Olivera, B. M. (2010) The tetrodotoxin receptor of voltage-gated sodium channels--perspectives from interactions with micro-conotoxins. *Mar Drugs* **8**, 2153-2161

19. Han, T. S., Zhang, M. M., Walewska, A., Gruszczynski, P., Robertson, C. R., Cheatham, T. E., 3rd, Yoshikami, D., Olivera, B. M., and Bulaj, G. (2009) Structurally minimized mu-conotoxin analogues as

sodium channel blockers: implications for designing conopeptide-based therapeutics. *ChemMedChem* **4**, 406-414

20. Khoo, K. K., Feng, Z. P., Smith, B. J., Zhang, M. M., Yoshikami, D., Olivera, B. M., Bulaj, G., and Norton, R. S. (2009) Structure of the analgesic mu-conotoxin KIIIA and effects on the structure and function of disulfide deletion. *Biochemistry* **48**, 1210-1219

21. Khoo, K. K., Gupta, K., Green, B. R., Zhang, M. M., Watkins, M., Olivera, B. M., Balaram, P., Yoshikami, D., Bulaj, G., and Norton, R. S. (2012) Distinct disulfide isomers of mu-conotoxins KIIIA and KIIIB block voltage-gated sodium channels. *Biochemistry* **51**, 9826-9835

22. Torres, F. S., Silva, C. N., Lanza, L. F., Santos, A. V., Pimenta, A. M., De Lima, M. E., and Diniz, M. R. (2010) Functional expression of a recombinant toxin - rPnTx2-6 - active in erectile function in rat. *Toxicon* **56**, 1172-1180

23. Leao, R. M., Cruz, J. S., Diniz, C. R., Cordeiro, M. N., and Beirao, P. S. (2000) Inhibition of neuronal high-voltage activated calcium channels by the omega-phoneutria nigriventer Tx3-3 peptide toxin. *Neuropharmacology* **39**, 1756-1767

24. Stevens, M., Peigneur, S., Dyubankova, N., Lescrinier, E., Herdewijn, P., and Tytgat, J. (2012) Design of bioactive peptides from naturally occurring mu-conotoxin structures. *J Biol Chem* **287**, 31382-31392

25. Wu\thrich, K. (1986) *NMR of proteins and nucleic acids*, Wiley, New York ; Chichester

26. Van Der Haegen, A., Peigneur, S., and Tytgat, J. (2011) Importance of position 8 in mu-conotoxin KIIIA for voltage-gated sodium channel selectivity. *FEBS J* **278**, 3408-3418

27. Brady, R. M., Zhang, M., Gable, R., Norton, R. S., and Baell, J. B. (2013) De novo design and synthesis of a mu-conotoxin KIIIA peptidomimetic. *Bioorg Med Chem Lett* **23**, 4892-4895

28. Walewska, A., Han, T. S., Zhang, M. M., Yoshikami, D., Bulaj, G., and Rolka, K. (2013) Expanding chemical diversity of conotoxins: peptoid-peptide chimeras of the sodium channel blocker mu-KIIIA and its selenopeptide analogues. *Eur J Med Chem* **65**, 144-150

29. Schroeder, C. I., Adams, D., Thomas, L., Alewood, P. F., and Lewis, R. J. (2012) N- and C-terminal extensions of mu-conotoxins increase potency and selectivity for neuronal sodium channels. *Biopolymers* **98**, 161-165

30. Walewska, A., Skalicky, J. J., Davis, D. R., Zhang, M. M., Lopez-Vera, E., Watkins, M., Han, T. S., Yoshikami, D., Olivera, B. M., and Bulaj, G. (2008) NMR-based mapping of disulfide bridges in cysteine-rich peptides: application to the mu-conotoxin SxIIIA. *J Am Chem Soc* **130**, 14280-14286

31. Zhang, M. M., Gruszczynski, P., Walewska, A., Bulaj, G., Olivera, B. M., and Yoshikami, D. (2010) Cooccupancy of the outer vestibule of voltage-gated sodium channels by micro-conotoxin KIIIA and saxitoxin or tetrodotoxin. *J Neurophysiol* **104**, 88-97

32. Lebbe, E. K., Peigneur, S., Brullot, W., Verbiest, T., and Tytgat, J. (2014) Ala-7, His-10 and Arg-12 are crucial amino acids for activity of a synthetically engineered mu-conotoxin. *Peptides* **53**, 300-306

33. Goral, R. O., Leipold, E., Nematian-Ardestani, E., and Heinemann, S. H. (2015) Heterologous expression of NaV1.9 chimeras in various cell systems. *Pflugers Arch* **467**, 2423-2435

34. Dib-Hajj, S. D., Black, J. A., and Waxman, S. G. (2015) NaV1.9: a sodium channel linked to human pain. *Nature reviews. Neuroscience* **16**, 511-519

35. Leipold, E., Markgraf, R., Miloslavina, A., Kijas, M., Schirmeyer, J., Imhof, D., and Heinemann, S. H. (2011) Molecular determinants for the subtype specificity of mu-conotoxin SIIIA targeting neuronal voltage-gated sodium channels. *Neuropharmacology* **61**, 105-111

36. Lewis, R. J., Dutertre, S., Vetter, I., and Christie, M. J. (2012) Conus venom peptide pharmacology. *Pharmacol Rev* **64**, 259-298

37. Markgraf, R., Leipold, E., Schirmeyer, J., Paolini-Bertrand, M., Hartley, O., and Heinemann, S. H. (2012) Mechanism and molecular basis for the sodium channel subtype specificity of micro-conopeptide CnIIIC. *Br J Pharmacol* **167**, 576-586

38. Green, B. R., Bulaj, G., and Norton, R. S. (2014) Structure and function of mu-conotoxins, peptide-based sodium channel blockers with analgesic activity. *Future Med Chem* **6**, 1677-1698

39. Akondi, K. B., Muttenthaler, M., Dutertre, S., Kaas, Q., Craik, D. J., Lewis, R. J., and Alewood, P. F. (2014) Discovery, synthesis, and structure-activity relationships of conotoxins. *Chem Rev* **114**, 5815-5847

40. Craik, D. J., Fairlie, D. P., Liras, S., and Price, D. (2013) The future of peptide-based drugs. *Chem Biol Drug Des* **81**, 136-147

41. Bhardwaj, G., Mulligan, V. K., Bahl, C. D., Gilmore, J. M., Harvey, P. J., Cheneval, O., Buchko, G. W., Pulavarti, S. V., Kaas, Q., Eletsky, A., Huang, P. S., Johnsen, W. A., Greisen, P. J., Rocklin, G. J., Song, Y., Linsky, T. W., Watkins, A., Rettie, S. A., Xu, X., Carter, L. P., Bonneau, R., Olson, J. M., Coutsias, E., Correnti, C. E., Szyperski, T., Craik, D. J., and Baker, D. (2016) Accurate de novo design of hyperstable constrained peptides. *Nature*

42. Hwang, T. L., and Shaka, A. J. (1998) Multiple-pulse mixing sequences that selectively enhance chemical exchange or cross-relaxation peaks in high-resolution NMR spectra. *J Magn Reson* **135**, 280-287

43. Spronk, C. A., Linge, J. P., Hilbers, C. W., and Vuister, G. W. (2002) Improving the quality of protein structures derived by NMR spectroscopy. *J Biomol NMR* **22**, 281-289

44. Liman, E. R., Tytgat, J., and Hess, P. (1992) Subunit stoichiometry of a mammalian K+ channel determined by construction of multimeric cDNAs. *Neuron* **9**, 861-871

45. Chan, L. Y., Gunasekera, S., Henriques, S. T., Worth, N. F., Le, S. J., Clark, R. J., Campbell, J. H., Craik, D. J., and Daly, N. L. (2011) Engineering pro-angiogenic peptides using stable, disulfide-rich cyclic scaffolds. *Blood* **118**, 6709-6717

46. Koradi, R., Billeter, M., and Wuthrich, K. (1996) MOLMOL: a program for display and analysis of macromolecular structures. *J Mol Graph* **14**, 51-55, 29-32

47. Davis, I. W., Leaver-Fay, A., Chen, V. B., Block, J. N., Kapral, G. J., Wang, X., Murray, L. W., Arendall, W. B., 3rd, Snoeyink, J., Richardson, J. S., and Richardson, D. C. (2007) MolProbity: all-atom contacts and structure validation for proteins and nucleic acids. *Nucleic Acids Res* **35**, W375-383

Figure Legends

Figure 1: Structure and sequence comparison of Pn. a) Superimposition of ten of the lowest energy structures. Superimposed across heavy backbone atoms for residues 4–12. Disulfide bonds (C1-C11 and C3-C13) are shown. **b)** Ribbon structure of a Pn representative structure showing all the side chains. **c)** Ribbon structure of KIIIA (PDB ID: 2LXG) highlighting pharmacophore residues. Positively charged residues are shown in blue, negatively charged residues are shown in red, hydrophobic residues are in green and disulfide bonds in orange. **d)** Sequence alignment and design strategy. Key residues for Na_V channel inhibition (green),

PnTx1 and KIIIA cysteines included in the design are shown in blue, and PnTx1 cysteines not included in the design strategy are highlighted in bold. PnM1-PnM9 (Series 1 and 2) include sequence variations compared to Pn, with mutations shown in red. PnCS1-PnCS4 (Series 3) peptides are cyclic variations of PnM9; mutations introduced for cyclisation purposes are shown in red. Disulfide bonds are shown in orange, dashed disulfide bond highlights the additional disulfide bond present in KIIIA compared to Pn. Backbone cyclisation is depicted with black lines, lactam-bond is shown in green and amidated C terminus is shown by *.

Figure 2: Electrophysiological profile of Pn on Navs. Superimposed current traces for the indicated Na_V isoforms before (black) and after application of 50 µM Pn. Currents were elicted by depolarizing pulses to 0 mV. The arrow indicates the peak current level in the presence of toxin; the dotted line indicates zero current level.

Figure 3: Electrophysiological characterization of Pn on $Na_V1.2$ channels. a) Steady-state activation and inactivation curves in control (closed symbols) and toxin conditions (50 µM Pn, open symbols). b) Competitive experiments to indicate that Pn does bind at site 1. Representative traces are shown in control (1); after application of 35 nM PnTx1 and after subsequently addition of 50 µM Pn.

Figure 4: Electrophysiological characterization of PnM9. a) Activity profile of PnM9 on Na_V channel isoforms. Representative whole-cell current traces in control and toxin conditions are shown. The dotted line indicates the zero-current level. The arrow marks steady-state current traces after application of 400 nM peptide. **b)** Concentration-response curves for $Na_V1.2$ channels indicating the concentration dependence of the Pn, PnM2 and PnM9-induced decrease of the Na^+ peak current.

Figure 5: Electrophysiological characterization of PnCS peptides. Activity profile of PnCS1 on Na_V channels. Representative whole-cell current traces in control and toxin conditions are shown. The dotted line indicates the zero-current level. The arrow marks steady-state current traces after application of 1 µM peptide. Black; current trace in control conditions, red, current trace in toxin situation.

Figure 6: Electrophysiological characterization of PnCS1 on $Na_V1.4$ channels. a) Steady-state activation and inactivation curves in control (black symbols) and toxin conditions (0.5 µM PnCS1, red symbols). No significant alteration of activation was noted. **b)** Normalized voltage-current relationship. **c)** Recovery from inactivation in control (closed symbols) and in the presence of 0.5 µM PnCS1 (open symbols). **d)** Voltage dependence of PnCS1 inhibition. No difference in the degree of inhibition was observed over a range of test potentials. **e)** Investigation of the state-dependence of inhibition was carried out and an expected degree of inhibition was observed after the 2 min incubation, indicating that the open state is not required for toxin interaction with the channel.

Figure 7: Serum-stability assay results. Percentage of peptide remaining in human serum in function of incubation time is shown.

Table 1: Structural statistics for the 20 Pn structures with best MolProbity scores.

Distance restraints	
Intra residue	78
Inter residue	46
Total	124
Dihedral angle restraints	0 (Not restrained)
Atomic RMSD (Å) [a]	
Mean global backbone (1–13)	2.89 ± 1.16
Mean global heavy (1–13)	4.35 ± 1.15
Mean global backbone (4–9)	1.41 ± 0.41
Mean global heavy (4–9)	3.31 ± 0.89
MolProbity Statistics[b]	
Clash score (>0.4 Å / 1000 atoms)	1.61 ± 2.53
Poor Rotamers	0.3 ± 0.47
Ramachandran Outliers (%)	11.82 ± 7.86
Ramachandran Favoured (%)	54.09 ± 11.61
MolProbity Score	1.91 ± 0.53
MolProbity Percentile[c]	75.60 ± 24.16

[a]RMSD. (46) [b]MolProbity.(47) [c]100th percentile is the best among structures of comparable resolution; 0th is the worst.

Table 2: Table with IC_{50} values in µM obtained for PnM1-4 on Na_V channel isoforms included in this study.

IC_{50} in µM	Nav1.2	Nav1.4	Nav1.5	Nav1.6
Pn	53.7 ± 3.2	n.a.	n.a.	n.a.
PnM1	6,4 ± 0,2	> 100	5,3 ± 0,6	2,2 ± 1,1
PnM2	1,8 ± 0,5	n.a.	10,4 ± 2,1	12,3 ± 1,8
PnM3	n.a.	n.a.	n.a.	n.a.
PnM4	n.a.	n.a.	n.a.	n.a.
PnM5	4,2 ± 0,4	8,3 ± 0,8	9,8 ± 1,1	27,4 ± 0,6
PnM6	31,7 ± 2,1	32,4 ± 2,1	> 100	> 100
PnM7	7,2 ± 0,1	3,1 ± 0,2	8,3 ± 2,1	n.d.
PnM8	3,7 ± 0,2	2,4 ± 0,1	> 100	n.d.
PnM9	0,3 ± 0,01	0,27 ± 0,1	> 100	56,3 ± 4,6

IC_{50} values of serie 1 mutants on several Nav channel isoforms. n.d. = not determinded, n.a. = no activity (at 100 µM), > 100 = IC50 value estimated above 100 µM.

Table 3: Table with IC_{50} values in µM obtained for PnCS1-4 on Na_V channel isoforms included in this study.

	PnCS1	**PnCS2**	**PnCS3**	**PnCS4**
$Na_V1.1$	0.8 ± 0.1	> 100	4.9 ± 0.4	1.1 ± 0.2
$Na_V1.2$	1.0 ± 0.1	> 100	5.3 ± 0.3	0.8 ± 0.1
$Na_V1.3$	1.1 ± 0.2	23 ± 1.6	5.4 ± 0.1	2.1 ± 0.6
$Na_V1.4$	0.6 ± 0.2	14.3 ± 1.4	10.7 ± 0.7	0.9 ± 0.2
$Na_V1.5$	2.8 ± 0.6	> 100	30.4 ± 4.5	4.5 ± 0.4
$Na_V1.6$	0.7 ± 0.2	> 100	4.5 ± 0.7	4.1 ± 0.6
$Na_V1.7$	0.9 ± 0.1	> 100	5.7 ± 0.2	3.1 ± 0.2
$Na_V1.8$	> 100	> 100	> 100	> 100
$Na_V1.9\_C4$	4.5 ± 0.4	> 100	23.8 ± 3.5	6.3 ± 0.4
$BgNa_V1.1$	n.a.	n.a.	n.a.	n.a.
VNa_V1	n.a.	n.a.	n.a.	n.a.
$DmNa_V1$	n.a.	n.a.	n.a.	n.a.

n.a.; not active

Figure 1.

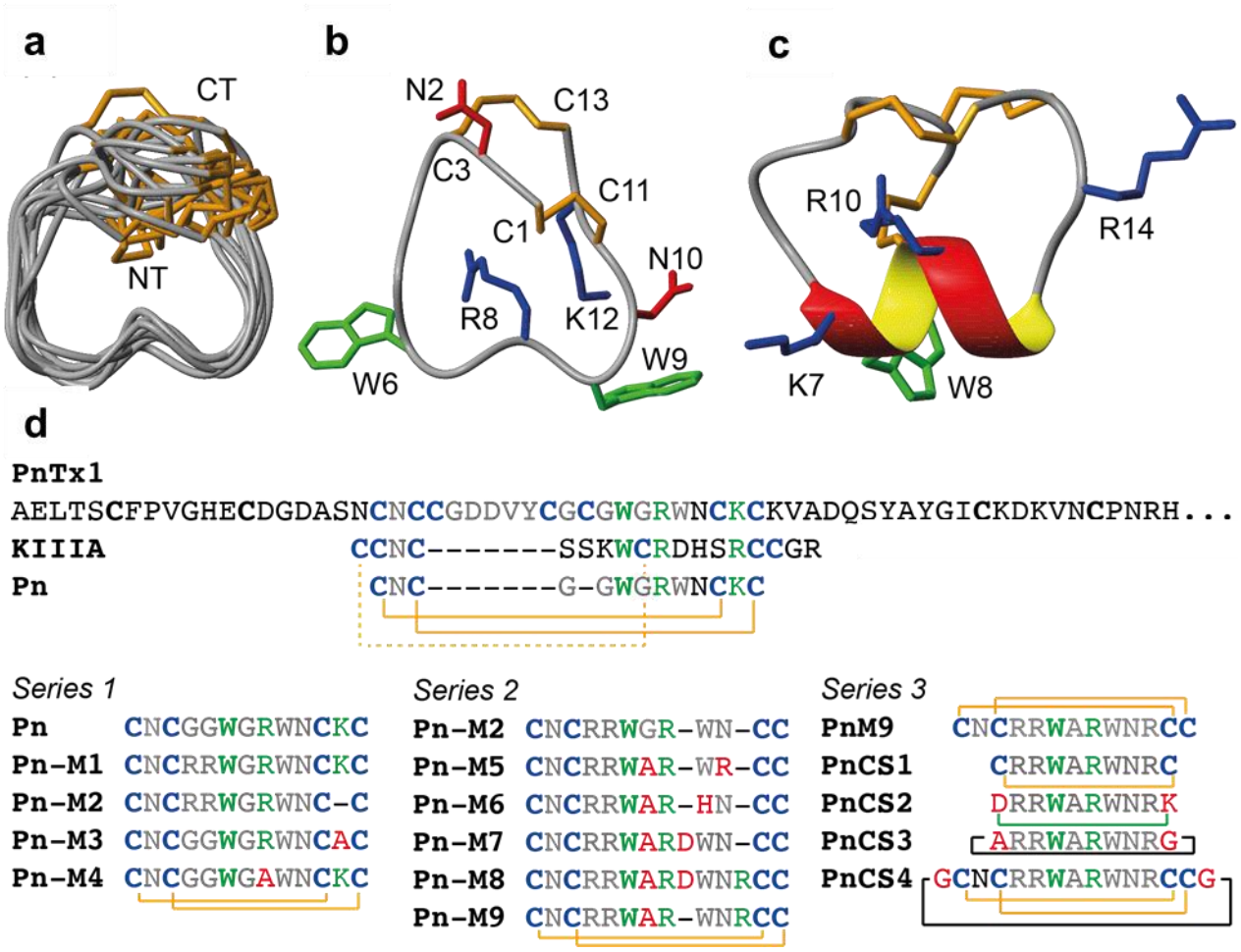

Figure 2.

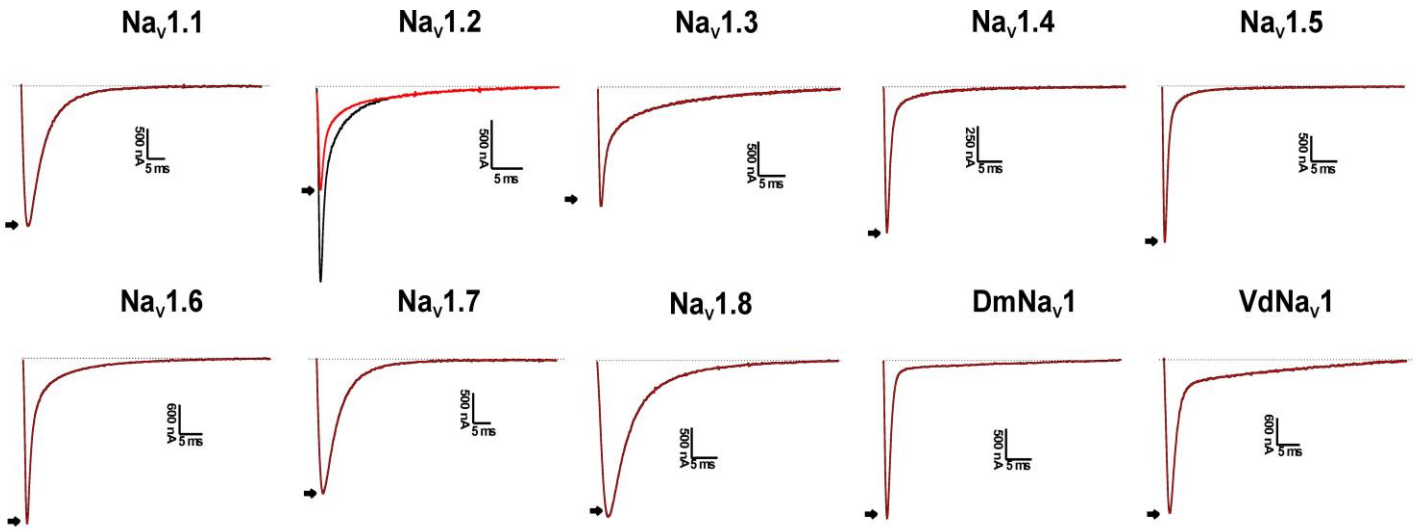

Figure 3.

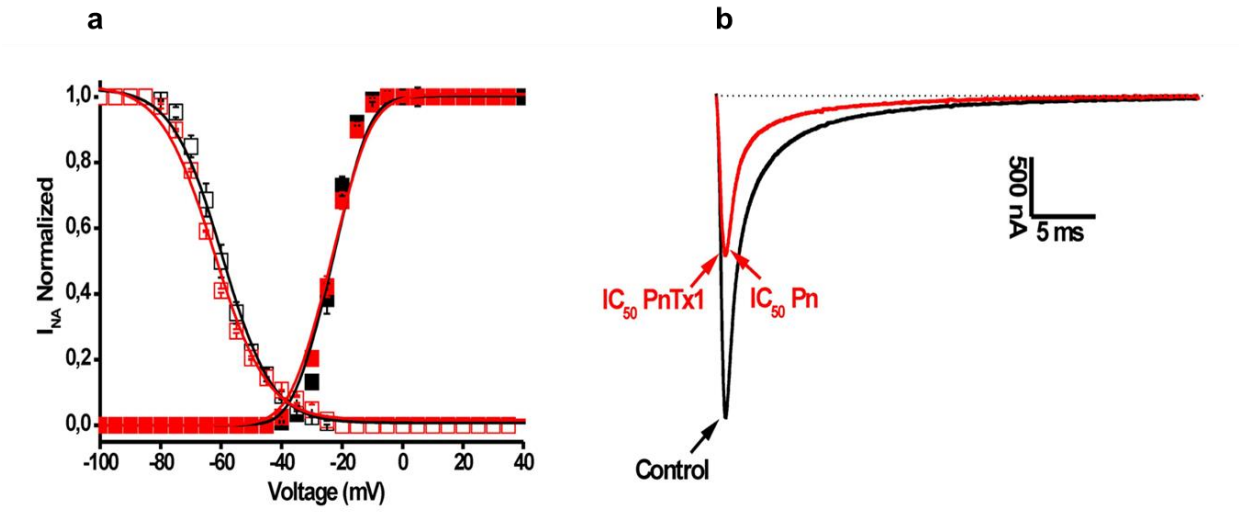

Figure 4.

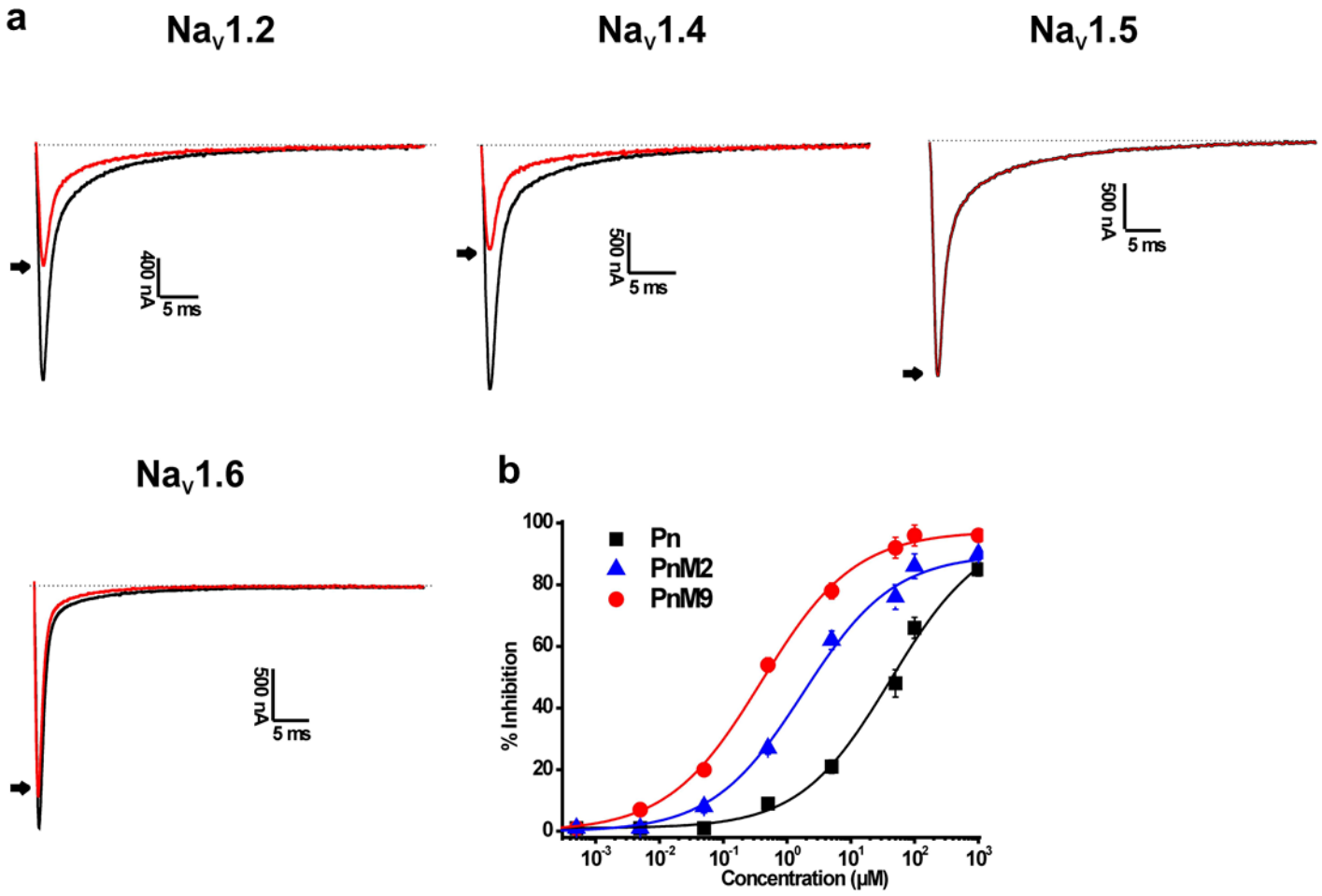

Figure 5.

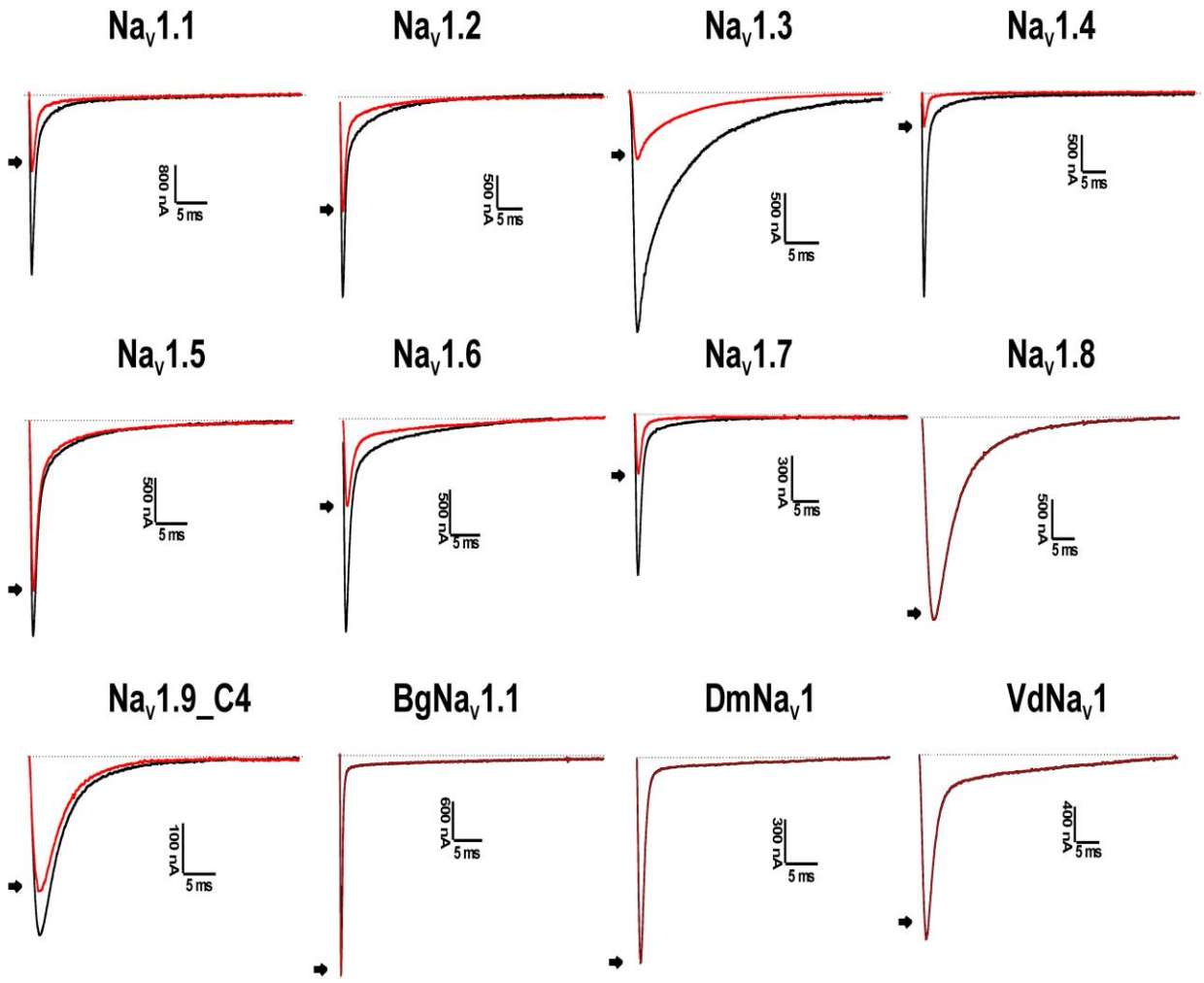
Na$_V$1.1
800 nA
5 ms
Na$_V$1.2
500 nA
5 ms
Na$_V$1.3
500 nA
5 ms
Na$_V$1.4
500 nA
5 ms
Na$_V$1.5
500 nA
5 ms
Na$_V$1.6
500 nA
5 ms
Na$_V$1.7
300 nA
5 ms
Na$_V$1.8
500 nA
5 ms
Na$_V$1.9_C4
100 nA
5 ms
BgNa$_V$1.1
600 nA
5 ms
DmNa$_V$1
300 nA
5 ms
VdNa$_V$1
400 nA
5 ms

Figure 6.

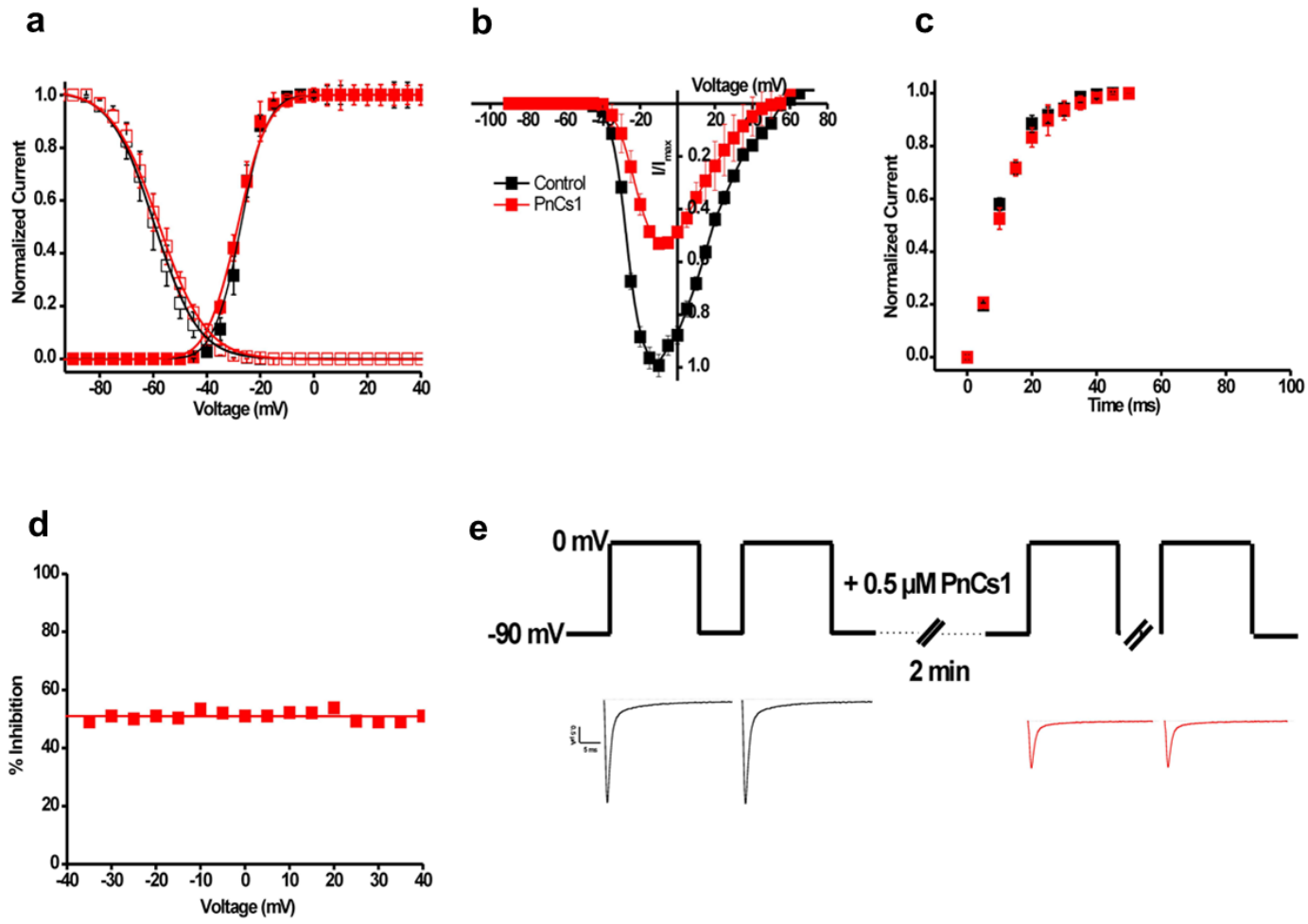
a
Normalized Current
Voltage (mV)
b
Voltage (mV)
Control
PnCs1
c
Normalized Current
Time (ms)
d
% Inhibition
Voltage (mV)
e
0 mV
-90 mV
+ 0.5 µM PnCs1
2 min

Figure 7.

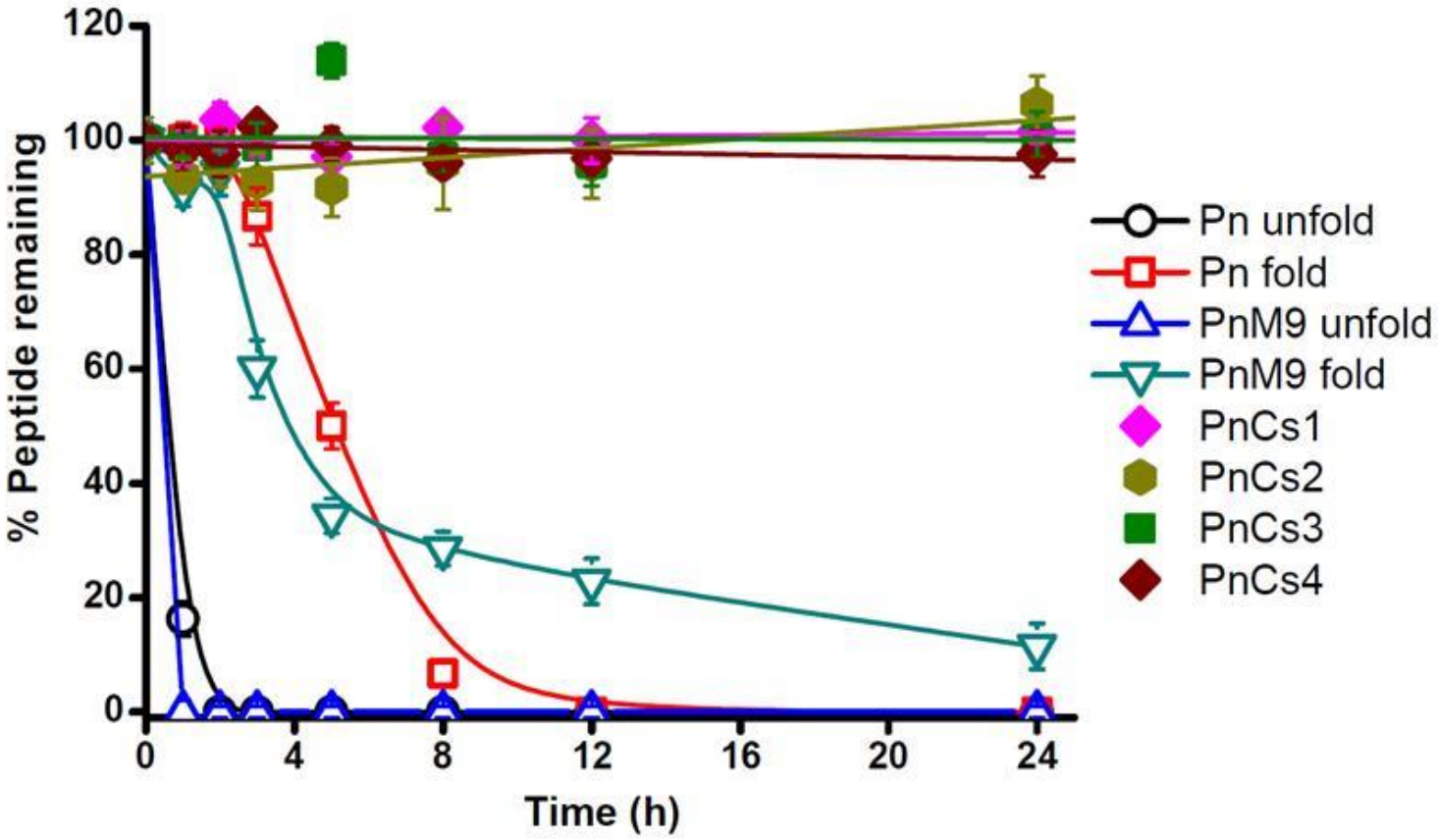
% Peptide remaining
120
100
80
60
40
20
0
0
4
8
12
16
20
24
Time (h)
Pn unfold
Pn fold
PnM9 unfold
PnM9 fold
PnCs1
PnCs2
PnCs3
PnCs4